

Effect of Temperature on the Nanomechanics of Lipid Bilayers Studied by Force Spectroscopy

Sergi Garcia-Manyes, Gerard Oncins, and Fausto Sanz

Department of Physical Chemistry, Universitat de Barcelona, 08028 Barcelona, Spain

ABSTRACT The effect of temperature on the nanomechanical response of supported lipid bilayers has been studied by force spectroscopy with atomic force microscopy. We have experimentally proved that the force needed to puncture the lipid bilayer (F_y) is temperature dependent. The quantitative measurement of the evolution of F_y with temperature has been related to the structural changes that the surface undergoes as observed through atomic force microscopy images. These studies were carried out with three different phosphatidylcholine bilayers with different main phase transition temperature (T_M), namely, 1,2-dimyristoyl-*sn*-glycero-3-phosphocholine, 1,2-dipalmitoyl-*sn*-glycero-3-phosphocholine, and 2-dilauroyl-*sn*-glycero-3-phosphocholine. The solid-like phase shows a much higher F_y than the liquid-like phase, which also exhibits a jump in the force curve. Within the solid-like phase, F_y decreases as temperature is increased and suddenly drops as it approaches T_M . Interestingly, a “well” in the F_y versus temperature plot occurs around T_M , thus proving an “anomalous mechanical softening” around T_M . Such mechanical softening has been predicted by experimental techniques and also by molecular dynamics simulations and interpreted in terms of water ordering around the phospholipid headgroups. Ion binding has been demonstrated to increase F_y , and its influence on both solid and liquid phases has also been discussed.

INTRODUCTION

Many efforts have been devoted to the study of physico-chemical properties (1) of lipid bilayers in recent years since they are crucial to understanding specific membrane function. Many of these structural and dynamic intrinsic bilayer properties such as the thickness of the bilayer, the area per lipid value, or the order parameter are governed by temperature (2). Indeed, lipid bilayers present many lamellar phases as a function of temperature, namely gel phase (L_β), liquid-crystalline phase (L_α), subgel phase (L_c), and ripple phase (P_β). It is widely accepted that many biologically relevant processes occur in the liquid-crystalline (L_α) phase, and therefore many works have focused on the study of structural and mechanical properties of this phase (2,3). Amid all the studies concerning phase transitions, the thermally induced gel-fluid transition has deserved special attention due to the large number of quantities that exhibit anomalous behavior near T_M , such as, e.g., heat capacity, ζ -potential (4), electric conductivity (5), Na^+ permeability (6), NMR order parameter (7), swelling (8), or hydration behavior (9). Most of those studies have been performed in multilamellar liposome solutions. In the case of supported planar phospholipid bilayers (SPBs), though, phospholipid molecules spontaneously adsorb to a planar solid support, thus creating a single lipid bilayer (10,11). In fact, SPBs are known to correctly mimic, up to an extent, complex biological membranes (12).

The atomic force microscope (AFM) has become an important tool to image supported thin films with nanometric

resolution. Concerning lipid bilayers, most of the studies have focused on resolving topographic characteristics in a liquid environment (13–22). With the possibility of accurately controlling temperature while scanning, a novel and promising research line has been opened, mainly devoted to studying topographic lipid bilayer surface features induced by temperature (23–28). Besides imaging, force spectroscopy allows us to obtain valuable experimental information about the interaction forces and mechanical behavior of the studied systems with nanometric and nanonewton resolution through the force-distance curves (29). When performing force curves in molecular thin films, a jump of the tip toward the surface is often observed once a threshold force has been exceeded. These jumps have also been observed in various systems such as surfactant layers on substrates (30), indicating tip penetration through the film, i.e., film rupture. Jumps on the force plots have also been observed when dealing with confined liquids, corresponding to a layer-by-layer tip penetration through the well-ordered squeezed liquid film (31–34) and also upon alkali halide single crystal nanoindentation, in which the tip penetrates the surface in a discrete layer-by-layer process (35). Recalling lipid bilayers, force curves have allowed us to obtain valuable information regarding phospholipid interaction forces, such as those generated either by Derjaguin-Landau-Verwey-Overbeek forces, by hydration forces, or by steric forces (36). Recent contributions have dealt with membrane nanomechanics using force spectroscopy, especially regarding the measurement of the elastic/plastic behavior of the bilayer as a function of its composition or the interaction with chemically modified probes (16,36,37). As in the case of other thin films, a jump on the approaching force curve has also been reported, this breakthrough being interpreted as the

Submitted May 2, 2005, and accepted for publication August 15, 2005.

Sergi Garcia-Manyes and Gerard Oncins contributed equally to this work. Address reprint requests to Fausto Sanz, Tel.: 34 934021240; Fax: 34 934021231; E-mail: fsanz@ub.edu.

© 2005 by the Biophysical Society

0006-3495/05/12/4261/14 \$2.00

doi: 10.1529/biophysj.105.065581

penetration of the AFM tip through the lipid bilayer (38). A quantitative measurement of the force at which the jump occurs can shed light onto gathering basic information concerning cell membrane nanomechanics as well as interaction forces between neighboring lipid molecules in the membrane. Therefore, the force value at which this jump takes place is closely related to membrane stability. So far, the dependence of the yield threshold force with the tip chemistry has been studied. It has been demonstrated that whereas hydrophilic tips yield a high material-dependent breakthrough force, hydrophobic tips give rise to a breakthrough force near the contact force (37). Besides, the approaching tip velocity has also been shown to have an effect on the force value at which the yield threshold occurs: the greater the tip approaching velocity, the higher the force within which the jump will occur, as a quantitative model predicts (39,40). Furthermore, in a recent work (1) we have shown that ionic strength increases the force at which the membrane breaks, probably due to ion binding on the phospholipid network, as a result of enhancing lateral interactions between neighboring molecules. This behavior was proved for model lecithin and phosphoethanolamine membranes as well as for natural membranes. Finally, in the framework of the same study, we correlated the yield threshold force with the chemical structure of both hydrophobic tails and hydrophilic heads. Likewise, the force at which this jump occurs can be regarded as a “fingerprint” of the bilayer stability under the experimental conditions in which the measurement is performed, just as force is the fingerprint for a protein to unfold or for a hard material surface to be indented. The yield threshold determination can then account for the overall forces that bind neighboring phospholipids together.

Temperature has a strong effect on lipid structure and stability. Therefore, the yield breakthrough, if present, should also present strong variations upon phase transition if it is really a direct mechanical reflection of molecular interactions. Although little work has been performed on this particular issue, it seems to be controversial (38) if the breakthrough can occur only in the solid-like phase (15) or the liquid-like phase (41). A pioneering meritorious publication (23) has suggested that the rupture force decreases as the temperature increases, but no quantitative experimental assessment has been reported.

In this work, we aim to perform a quantitative study of the dependence of the yield threshold force on model lipid bilayers with temperature and to relate the results with the structural changes that the surface undergoes as studied through AFM images. In particular, our first goal is to study whether the jump occurs in the gel phase, in the liquid phase, or in both. To this aim we have performed the same experiment with three different phosphatidylcholine phospholipids that exhibit a well-reported different main transition temperature, namely, 1,2-dipalmitoyl-*sn*-glycero-3-phosphocholine (DPPC), 1,2-dimyristoyl-*sn*-glycero-3-phosphocholine

(DMPC), and 2-dilauroyl-*sn*-glycero-3-phosphocholine (DLPC). An in-depth study of the evolution of the yield threshold with temperature can shed light onto understanding the temperature-induced changes in the intermolecular interactions between the phospholipid molecules, which is crucial to many biological functions.

MATERIALS AND METHODS

Sample preparation

DMPC (Sigma, St. Louis, MO; >98%) was dissolved in chloroform/ethanol (3:1) (Carlo Erba, Milan, Italy; analysis grade, at 99.9%) to give a final DMPC concentration of 2 mM. This solution was kept at -10°C . A $500\ \mu\text{l}$ aliquot was poured into a glass vial, and the solvent was evaporated with a nitrogen flow, obtaining a DMPC film at the bottom of the vial. Solution was kept in vacuum overnight to ensure the absence of organic solvent traces. Then, water solution was added until a final DMPC concentration of $500\ \mu\text{M}$ was obtained. Because of the low solubility of DMPC in water, the vial was subjected to 30 s cycles of vortexing, temperature, and sonication until the mixture was homogeneous. The solution was finally sonicated for 20 min (to have unilamellar liposomes) and allowed to settle overnight always protected from light and maintained at 4°C . Lipid resuspension was carried out by using either a high ionic strength solution ($150\ \text{mM NaCl} + 20\ \text{mM MgCl}_2$) or only distilled water. All solutions used in this work were set at $\text{pH} = 7.4$ with $10\ \text{mM Hepes/NaOH}$. Before its use, mica surfaces (Metafix, Montdidier, France) were glued onto Teflon discs with a water insoluble mounting wax. A total of $50\ \mu\text{l}$ of DMPC, DLPC, or DPPC dissolution at the specific ionic strength was applied to cover $0.5\ \text{cm}^2$ freshly cleaved pieces of mica for a deposition time of 35 min. After that, mica was rinsed three times with $100\ \mu\text{l}$ of the corresponding ionic aqueous solution. The process of vesicle formation and deposition for the rest of the phospholipid bilayers used in this work's DLPC and DPPC (all of them from Sigma >98%) is the same as the one described for DMPC. In the case of DPPC, however, the temperature cycles for resuspension were set to $\sim 50^{\circ}\text{C}$ due to the higher T_M for this phospholipid.

DSC measurements

Differential scanning calorimetry (DSC) measurements were performed with a MicroCal MC-2 (MicroCal, Northampton, MA). The heating and cooling rate was usually $10^{\circ}\text{C h}^{-1}$, and the measurements were performed in the temperature interval from 10°C to 55°C . The reproducibility of the DSC experiments was checked by three consecutive scans of each sample.

Temperature-controlled AFM imaging

AFM images were acquired with a Multimode (Digital Instruments, Santa Barbara, CA) microscope equipped with a J-Scanner AS 130V with fluid heat exchanger controlled by a Nanoscope IV electronics (Digital Instruments) in contact mode using V-shaped Si_3N_4 tips (OMCL TR400PSA, Olympus, Tokyo, Japan) cantilevers. The applied force when obtaining topographic images was controlled by acquiring force plots before and after every image was captured so as to measure the force increment from the set point value. Temperature-controlled experiments were performed with a temperature controller stage (high temperature heater controller: range: up to 250°C , resolution: 0.1°C , accuracy: 3%, temperature drift: $\pm 0.25^{\circ}\text{C}$; Digital Instruments). Basically, the temperature setup consists of a resistor placed between the scanner and the sample that transmits the heat to the sample from underneath. The piezo is always kept under its Curie temperature by a cooler fluid circuit. This applied temperature is the temperature that the heater displays as the “sample temperature” and the temperature that indeed has been used in most of the AFM-controlled studies

as the sample temperature. However, in conventional AFM imaging in a liquid environment, the mica sample is glued to a thin Teflon disk that is glued to a metallic holder. The whole sample remains attached to the microscope scanner by a magnet. Although the distance between the heating element and the sample itself (inside the buffer droplet) is typically $<3\text{--}4$ mm, the temperature gradient between the displayed and the real temperature is substantial (Fig. S1 in the Supplementary Material) and varies (up to $\sim 25\%$ at high temperatures) for different Teflon holders that differ only 1 mm in height. Therefore, calibration of individual sample holders becomes compulsory. Sample temperature is measured by a thermocouple (Cole Palmer (Vernon Hills, IL) thermocouple thermometer EW-91100-20 Digi Sense: resolution: 0.1C, accuracy: $\pm 0.25\%$ provided with Omega (Brattleboro, VT) precision fine wire thermocouples) that measures the temperature inside the buffer droplet just in contact with the sample surface. Upon imaging, temperature was varied from 16°C up to 85°C with a $0.5^\circ\text{C}/\text{min}$ ramp. Before every image was acquired, a dwell time of 4–5 min lapsed to let the system equilibrate temperature. However, temperature equilibration was measured to be typically <45 s.

Force spectroscopy

Force spectroscopy was performed with the same setup using the force-extension mode. Force plots were acquired using V-shaped Si_3N_4 tips (OMCL TR400PSA, Olympus) with a nominal spring constant of 0.08 N/m when performing force curves on DLPC and DMPC and V-shaped Si_3N_4 tips (tip ‘‘F’’, Thermomicroscope, Sunnyvale, CA) with a nominal spring constant of 0.5 N/m when performing force plots on DPPC (higher yield threshold values (1)). Individual spring constants were calibrated using the equipartition theorem (thermal noise) (42) after having correctly measured the piezo sensitivity (V/nm) by measuring it at high voltages after several minutes of performing force plots to avoid hysteresis. It has to be pointed out that the results here shown within the same experiment were obtained with the same cantilever keeping the spot laser at the same position on the lever to

avoid changes in the spring constant calculation (43). However, results have low scattering when using different tips and different samples (within 10% error). Tip radius was individually measured by imaging a silicon grating (MikroMasch (Tallinn, Estonia), Ultrasharp TGG01, silicon oxide $3\ \mu\text{m}$ pitches). Individual radii were found to be 30 ± 10 nm, although little variation $<20\%$ was found for tips from the same wafer; ~ 300 curves were obtained for each temperature. All experiments were performed at the same indenting velocity ($1\ \mu\text{m}/\text{s}$) so that the small effect of the velocity on the breakthrough force could be totally neglected. Applied forces, F , are given by $F = k_c \times \Delta$, where Δ is the cantilever deflection and k_c is the cantilever spring constant. The surface deformation is given as penetration (δ) evaluated as $\delta = z - \Delta$, where z represents the piezo-scanner displacement. X -, Y -, Z - piezo motion was calibrated with a Digital Instruments silicon oxide grid (STR10-1800P), 180 nm deep, $10\ \mu\text{m}$ pitch.

RESULTS

Topographic evolution of a supported DMPC bilayer with temperature

Liposome deposition onto hydrophilic, negatively charged surfaces such as mica has been proved to be electrostatically governed: high ionic strength solutions give rise to compact, huge planar bilayers extending some micrometers, whereas under distilled water small discontinuous islands are formed (1). This is the main reason we have chosen to mainly work under high ionic strength conditions, since under these conditions the huge, completely formed bilayers allow us to follow the topography changes as the temperature is varied in a reproducible way. The evolution of the topography of a

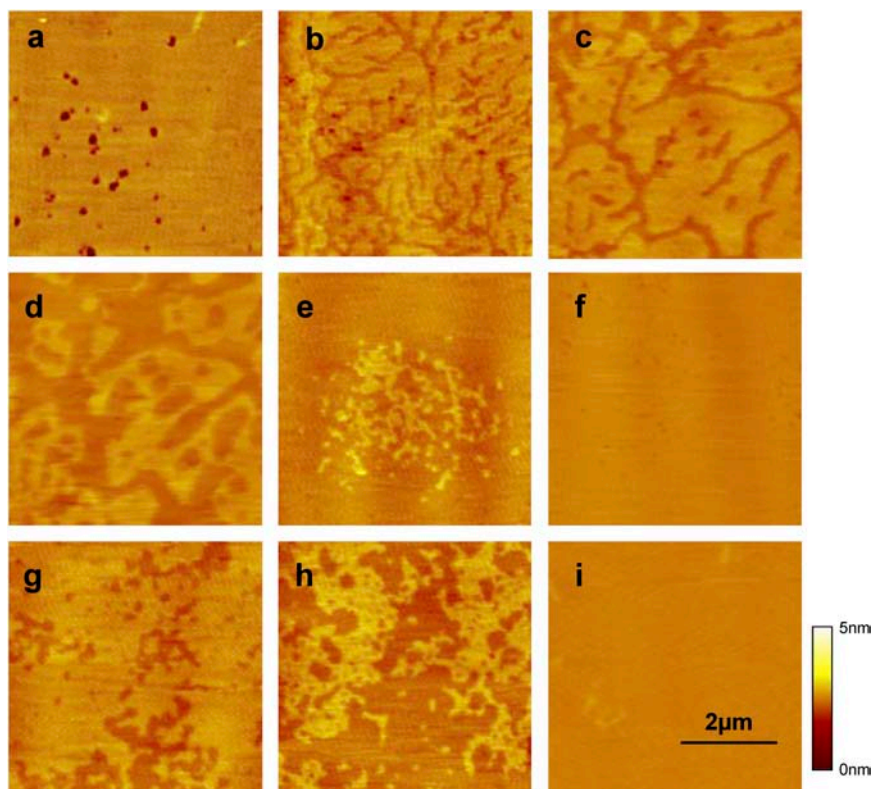


FIGURE 1 AFM contact mode images showing the phase transition for a DMPC-supported bilayer upon heating the sample (a) 19.0°C , (b) 24.4°C , (c) 27.2°C , (d) 28.3°C , (e) 29.3°C , (f) 30.3°C , (g) 31.3°C , (h) 32.9°C , and (i) 37.5°C . All images were acquired by applying a constant force of 1.5–2 nN.

DMPC bilayer from room temperature to 50°C is shown in Fig. 1 upon $5 \times 5 \mu\text{m}^2$ contact mode AFM images under high ionic strength conditions, which yield well-defined supported lipid single bilayers (1). At 19°C (Fig. 1 *a*) the gel phase (L_β) is observed. The black holes (defects in the bilayer) correspond to the mica support. From cross sections (see Fig. 2) the width of the bilayer can be measured to be 5 ± 0.3 nm, which corresponds to the height of a single supported bilayer (the fully hydrated DMPC bilayer is found to measure 5.99 nm at 10°C (44)). When increasing temperature up to 22°C (in all cases the registered temperature is the “real” temperature, lower than the temperature externally applied to the system, see the Materials and Methods section) ruptures on the extended L_β phase are observed. The initial temperature at which the first hint of phase transition is observed is in good accordance with the DSC main transition temperature peak (23.6°C, Fig. 2). Those lines, 0.5 ± 0.1 nm lower than the L_β surface, become wider as the temperature is increased, thus showing clear phase separation (Fig. 1 *b*, $T = 24.4^\circ\text{C}$). The high domain corresponds to the remaining L_β phase and the low domain to the fluid-like L_α phase. Further increasing the temperature leads to an increased progressive disappearance of the L_β phase (Fig. 1 *c*, $T = 27.2^\circ\text{C}$; Fig. 1 *d*, $T = 28.3^\circ\text{C}$) until the whole surface is covered by the fluid-like phase (Fig. 1 *f*, $T = 30.3^\circ\text{C}$). Therefore, the whole main transition is observed within $\sim 5.5^\circ\text{C}$. The broader T_M width observed upon supported bilayers related to that observed in unilamellar vesicles in solution through DSC experiments might be due to the single bilayer nature of the SPB and to the substrate effect (23). Interestingly, upon further increasing temperature a new

phase separation is observed (Fig. 1 *g*, $T = 31.3^\circ\text{C}$). These two different phases have a difference of 0.6 ± 0.1 nm in height. The total height with respect to the mica surface cannot be assessed due to the lack of defects. The temperature gap that comprises the whole disappearance of the upper L_α phase ranges from 32.9°C (Fig. 1 *h*) to 37.5°C (Fig. 1 *i*). At higher temperatures (up to 80°C) no further topographic changes were observed. A complete sequence of evolution of the same scanned surface area is provided in the Supplementary Material (Fig. SI2). Interestingly, the results concerning the evolution of the bilayer topography with temperature when measured under distilled water are basically the same as those observed under high ionic strength conditions. Nonetheless, under distilled water the phase transitions are not as clear as in the case of high ionic strength conditions because the islands are too small to assess a particular temperature the moment at which the transition starts. In any case, the temperature gap is still $\sim 14^\circ\text{C}$ to reach unambiguously the liquid phase upon raising the temperature. The first observed transition clearly corresponds to the gel phase-fluid phase ($L_\beta \rightarrow L_\alpha$) transition, and it is in perfect accordance with the main transition temperature peak observed upon DSC measurements. However, the nature of the second observed phase transition is unclear. Two possible explanations could account for the experimental observations. On the one hand, as stated in Leonenko et al. (23), this second transition could be associated with the formation of a fluid-disordered phase, perhaps with interdigitated or partially interdigitated lipid chains, but this new phase is not observed upon lipid bilayer extensive available literature or in our DSC measurements.

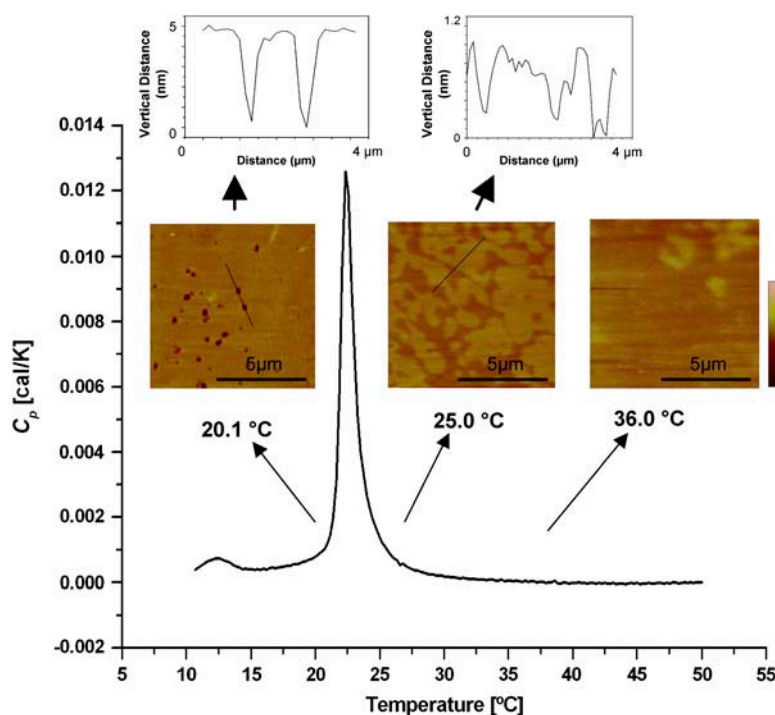


FIGURE 2 DSC register obtained in a DMPC unilamellar liposome solution under the same high ionic strength solution used upon AFM images and force spectroscopy experiments (150 mM NaCl + 20 mM MgCl_2 , pH = 7.4). The plot shows a peak centered at 23.6°C corresponding to the lipid main phase transition. In contrast, $10 \times 10 \mu\text{m}^2$ contact mode AFM images show the topography of the supported bilayer before (20.1°C), during (25°C), and after (36°C) the main phase transition. Although the main $L_\beta \rightarrow L_\alpha$ transition occurs within $\sim 3^\circ\text{C}$ in solution, the temperature range broadens up to $\sim 14^\circ\text{C}$ when supported in mica.

On the other hand, the two observed transitions could belong to the same ($L_\beta \rightarrow L_\alpha$) transition after the decoupling of the phase behavior of the two leaflets of mica-supported PC bilayers as proposed upon the DSC results obtained on mica-supported bilayers (45). This finding would support the theory that the coupling between the two leaflets in a unique bilayer is weak (46). As it has been pointed out in Yang and Appleyard (45), the effect due to the substrate-lipid interaction may be stronger than the interaction between leaflets, so the higher temperature transition would be due to the DMPC leaflet in contact with mica. This behavior highlights the fact that the actual temperature at which the main phase transition takes place is also highly sensitive to the environment surrounding the bilayer. This possibility was excluded in Leonenko's et al. (23) interpretation, since this would lead to more than two domains of different thickness at intermediate temperatures and instead only two domains at a time have been observed. The only possibility is then that one leaflet melts completely before the other starts to melt. Indeed, we do not exclude such possibility. Further investigation involving Langmuir-Blodgett monolayers may shed light on this issue. Finally, a third interpretation concerning the possibility of having a multibilayer instead of a single bilayer deposited on the surface and therefore the two-step gel-fluid phase transition being associated to the presence of a first bilayer sticking on the mica support and the second transition being related to the second bilayer, less affected by this support, has been excluded. Several reasons support this belief. First, upon AFM images we realize that the depth between the bilayer surface (brighter regions) and the substrate (darker regions) is ~ 4.5 nm, which is the depth of a single bilayer (also related to the width of the jump observed upon force spectroscopy measurements). Moreover, we can assess that there is not evidence of a first bilayer stacked on the surface since lateral force microscopy studies reveal the presence of a single bilayer deposited on the mica surface (47). Indeed, lateral force profiles show a clearly different behavior in the bilayer (also related with a discontinuity in the lateral force plot) and in the mica substrate. Furthermore, the probability of having a double bilayer is much higher in PE membranes than in the case of PC membranes, where the deposition of a second PC bilayer on a first deposited bilayer is not favored (17). Therefore, for the reasons outlined above, we tend to think that we only have a single bilayer deposited on the surface.

In any case, it is clear that below 23°C only the solid-like phase is present in the system, and above 37°C the whole surface is covered by the liquid-like phase. These considerations have to be taken into account for further discussion in the forthcoming lines. Finally, the evolution of the bilayer topography has been performed upon cooling the system from 45°C to ambient temperature. The process appears to be reversible, since the phases observed during heating are recovered while cooling down to the initial temperature.

Fig. 2 shows a summary of the surface topography characteristics as a function of temperature before and after the main transition temperature. The DSC thermogram has been acquired for unilamellar liposomes under the same high ionic strength solution used upon AFM imaging and force spectroscopy measurements, and it shows a main peak corresponding to the ($L_\beta \rightarrow L_\alpha$) transition at $23.6^\circ\text{C} \pm 1^\circ\text{C}$. The same transition has been shown upon AFM images (Fig. 1) to occur within a wide range of temperatures, namely, 23°C – 37°C . At temperatures below the main phase transition (20.1°C), the bilayer surface looks compact. The small holes serve to measure the bilayer height (in this particular case, of 4.7 nm). Just after the main transition temperature (25.0°C), the phase has totally changed from the L_β phase into the L_α phase in solution, as can be seen from the DSC register, but two domains of different height $\Delta h \sim 0.6$ nm (cross section) are observed in supported bilayers. The whole transition is over at 36°C , after the second transition has taken place. Therefore, whereas the main transition takes place in solution within a temperature range of $\sim 3^\circ\text{C}$ (DSC register), the transition temperature range broadens up to $\sim 14^\circ\text{C}$ when phospholipids bilayers are surface supported. Here it is worth pointing out that according to our data and also on account of the results available in the literature (48,49), increasing ionic strength gives rise to an increase in the T_M determination by DSC measurements in solution. In our case, this shift is $\sim 0.3^\circ\text{C}$ upon DSC measurements, but unfortunately this variation is difficult to assess when the bilayers stand supported on a substrate, especially due to the fact that under water, lipid bilayers do not form a continuous, huge bilayer as stressed above. An in-depth molecular dynamics (MD) study concerning a finite number of phospholipid and water molecules dealing with the evolution of the interactions arising between them while varying the temperature would help us to understand the underlying processes from an atomistic point of view.

Force spectroscopy on a supported DMPC bilayer

As above stated, lipid bilayers are shown to present a discontinuity in the force plot, this jump being related to the tip penetration into the bilayer. The force at which this jump occurs is the maximum force that the membrane is able to withstand before the onset of plastic deformation occurs, and it is a reflection of the lateral forces that bind the phospholipid molecules together. The question remains open, however, of whether it is only the solid (gel) phase that can be punctured with the AFM tip or if, in addition, the liquid phase also shows a jump in the force curve. Since 1,2-dioleoyl-3-trimethylammonium-propane (DOTAP), ($T_M = 0^\circ\text{C}$) (39,41), and 1,2-dioleoyl-*sn*-glycero-3-[phospho-L-serine] (DOPS), ($T_M = -11^\circ\text{C}$) (38,39), bilayers have been punctured and we have recently observed jumps when indenting 1,2-dioleoyl-*sn*-glycero-3-phosphocholine (DOPC) ($T_M = -20^\circ\text{C}$) and DLPC ($T_M = -1^\circ\text{C}$) bilayers

(1), it seems clear that the liquid phase presents enough ordering and cohesion (jumps are related to molecular ordering (50)) to show the breakthrough. Then, the real challenging point to be addressed is the evolution of the yield threshold force with temperature. To deal with this question we have formed a DMPC bilayer onto a freshly cleaved mica surface. A 200–300 μl buffered water droplet was deposited onto the sample, and the surface was imaged to check the presence of the bilayer. Continuous bilayer regions of $>40\ \mu\text{m}$ were easily created after long deposition times ($\sim 35\ \text{min}$) in high ionic strength solutions. Once a good bilayer region was chosen, a set of 300 consecutive force plots over different places of the sample was performed. Interestingly, $\sim 80\%$ of the force curves presented the jump, which implies that bilayers self-heal within the time of two successive force plots. In $\sim 12\text{--}15\%$ of the force plots, especially when conducted under high ionic strength conditions, a double jump in the force curve was observed. This second jump was interpreted as a lipid bilayer formed on the AFM tip (51) and was closely related to the presence of high ionic strength conditions. No relationship between the presence of such second jumps and temperatures has been observed. The recordings where two jumps have been observed have been excluded for data statistics. After having performed the force plots, the heater temperature was raised 5°C . Then, after waiting $\sim 4\text{--}5\ \text{min}$ for temperature equilibration, another set of 300 curves was performed. This process was repeated from ambient temperatures up to $\sim 70^\circ\text{C}\text{--}80^\circ\text{C}$. The setup was kept under high humidity conditions throughout the experiment. Fig. 3 shows four force curves obtained at different temperatures: (a) 22°C , (b) 29.5°C , (c) 40.9°C , and (d) 52.4°C . The jump is clearly observed as a discontinuity in the force plot, and it occurs at $\sim 11.0\ \text{nN}$ (a), at $\sim 5.5\ \text{nN}$ in (b), at $\sim 6.2\ \text{nN}$ (c), and at $\sim 5.8\ \text{nN}$ (d). A statistical data treatment has been performed by fitting a Gaussian distri-

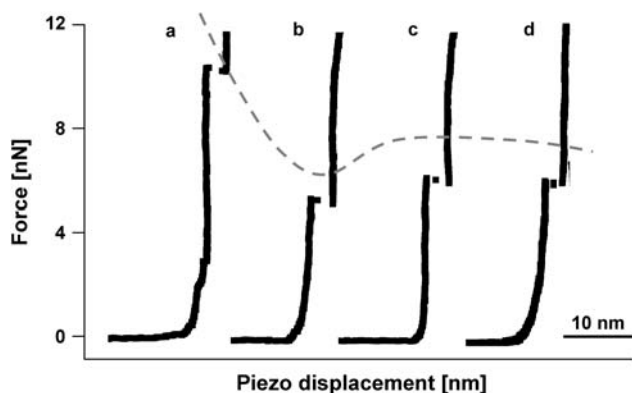


FIGURE 3 Force-distance curves obtained on a DMPC-supported lipid bilayer at different temperatures: (a) 20.1°C , (b) 29.5°C , (c) 40.9°C , and (d) 52.4°C . The discontinuity in the force-distance curve (breakthrough) indicates the tip penetration into the lipid bilayer, and the force at which it takes place is called yield threshold force. The dotted line highlights the overall breakthrough tendency as the temperature is increased.

bution to the histogram of the breakthrough forces obtained for each sampled temperature. The dotted line highlights the overall breakthrough force tendency as temperature is increased. Fig. 4 shows the evolution of the yield threshold

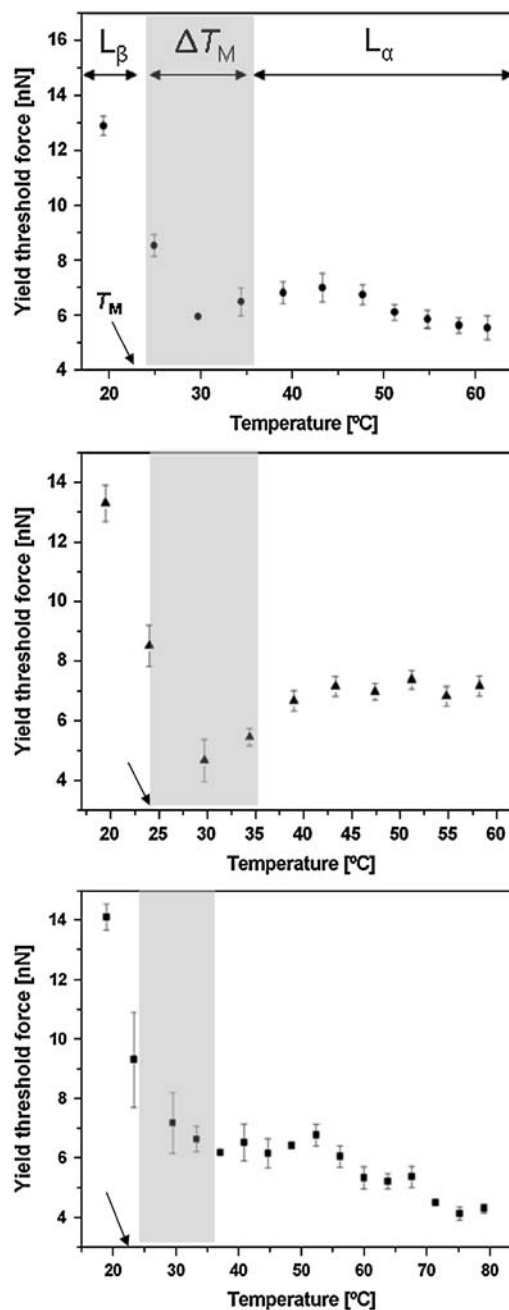


FIGURE 4 Yield threshold force dependence of a mica-supported DMPC bilayer with temperature for three independent experiments (different tip, different sample). All measurements were performed under high ionic strength solution. Each point in the graph corresponds to the center value of a Gaussian fitting to the obtained histogram. Error bars stand for standard deviation of the Gaussian fitting to the yield threshold force histograms. T_M stands for the main transition temperature obtained from DSC measurements. Dark areas stand for the temperature range (ΔT_M) in which phase transitions are observed in supported planar bilayers through AFM images (Fig. 1).

force for three independent experiments (different tip, different sample). Each point in the graph corresponds to the Gaussian center \pm standard deviation. As can be observed, the yield threshold force occurs at $\sim 13\text{--}15$ nN for temperatures around 20°C . This is in accordance with the results obtained in Garcia-Manyes et al. (1) for DMPC under high ionic strength (14.93 ± 0.09 nN). As temperature is increased, the yield threshold value occurs at lower force, and it reaches a minimum in force at $\sim 25\text{--}33^\circ\text{C}$ ($\sim 4.5\text{--}6$ nN). This temperature range corresponds to the phase transitions observed in supported bilayers, as AFM images reveal (Fig. 1). Still, in every force plot the jump is observed, thus suggesting that even though the yield threshold force has sensibly decreased, the membrane has not lost its compactness. Further increasing temperature leads to an increase in the yield threshold force, up to ~ 7 nN. When temperature is further raised, it results in a more or less constant yield threshold force or even in a slight decrease in the breakthrough force, especially for temperatures $>60^\circ\text{C}$. Therefore, the general picture of the process yields a high yield force value for temperatures below T_M and a sudden decrease in force at temperatures around T_M , thus creating a “well” in the plot around T_M . In each plot in Fig. 4 the dark area region corresponds to the temperature range in which the main transition phase has been observed upon contact images, thus highlighting the correspondence between the surface phase transition regime and the force well observed through force spectroscopy results. Upon rising

temperature, the yield force rises again until a more or less stable value within the liquid-like phase.

DMPC is a good candidate to study its nanomechanical response within both solid-like and fluid-like phases and especially around the main transition temperature since its T_M value, 23°C , and its expanded range $23^\circ\text{C}\text{--}36^\circ\text{C}$ when bilayers are supported lies within ambient temperatures. Yet it does not allow studying the yield threshold evolution with temperature within the gel phase. To this aim we have performed the same experiment with DPPC, which only differs from DMPC in two more $-\text{CH}_2$ groups in both hydrophobic tails, which implies a higher T_M , $\sim 41^\circ\text{C}$ (45).

Topographic evolution of a DPPC bilayer with temperature

Fig. 5 shows the evolution of the surface topography with temperature. At room temperature (well below the T_M) (24.5°C , Fig. 5 *a*), the surface looks like the gel-phase observed for DMPC (Fig. 1 *a*). Many “holes” or defects can be observed, which allow us to measure the bilayer height (~ 5.1 nm). Those holes do not heal or disappear while continuously scanning the surface in contact mode at this temperature. However, as temperature is raised (Fig. 5 *b*, 37.7°C) the number of defects is greatly reduced until they completely disappear (Fig. 5 *c*, 38.7°C), thus implying a lateral expansion (increase in the area/lipid value) of the phospholipid molecules in the gel phase. At 44.8°C (Fig. 5 *d*)

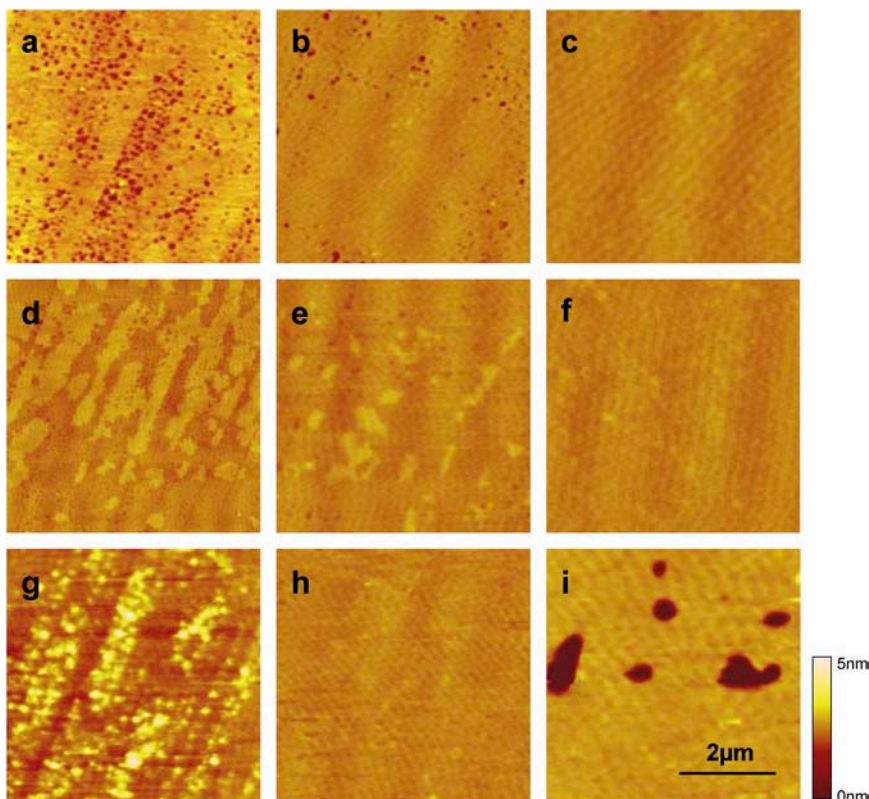


FIGURE 5 AFM contact mode images showing the main phase transition for a DPPC-supported bilayer upon heating the sample (*a*) 24.5°C , (*b*) 37.7°C , (*c*) 38.7°C , (*d*) 44.8°C , (*e*) 48.3°C , (*f*) 51.4°C , (*g*) 52.9°C , (*h*) 59.4°C , and cooling back to (*i*) 34.2°C .

the L_β phase starts to separate from the lower fluid-like L_α phase. This L_α phase expands as temperature is increased (Fig. 5 e, $T = 48.3^\circ\text{C}$) until the total disappearance of the L_β phase (Fig. 5 f, $T = 51.4^\circ\text{C}$), thus implying that the whole surface is covered by the fluid-like phase. On further heating the sample, the liquid-like phase is being disrupted (Fig. 5 g, 52.9°C) by the appearance of a lower phase, which expands and finally totally covers the surface (Fig. 5 h, 59.4°C). Finally, upon cooling the system back to 34.2°C , the surface recovers its compact, initial L_β phase (Fig. 5 i). Interestingly, the solid-like phase obtained after a heating-cooling process looks typically much more compact than the initial L_β phase, perhaps on account of the better rearrangement of phospholipids due to the temperature effect; in this case, the number of defects or holes is typically smaller even though they are bigger than those observed in the initial L_β phase (Fig. 5 a). Regarding the main phase transition, it occurs $44.8\text{--}51.5^\circ\text{C}$ (first transition) and $52\text{--}59^\circ\text{C}$ (second transition). Regardless of whether both are considered to be part of the $L_\beta \rightarrow L_\alpha$ transition (separate temperature ranges for both bilayer leaflets) or the second transition being related to the formation of a fluid-disordered phase, it is clear that phase transition occurs in surface within a range of $\sim 15^\circ\text{C}$, i.e., $45\text{--}60^\circ\text{C}$. Overall, the observed process is in the case of DPPC very similar to that observed by Leonenko et al. (23).

Force spectroscopy on a DPPC bilayer

Once the surface topographic characteristics and their dependence with temperature were well known, we performed a force spectroscopy experiment analogous to that performed with DMPC. The evolution of the yield threshold force with temperature for two independent experiments is shown in Fig. 6. At low temperature ($\sim 24^\circ\text{C}$) the yield threshold force was found to be $\sim 23\text{--}26\text{ nN}$, which is again in very good accordance with the results obtained in Garcia-Manyes et al. (1). Here we have to outline the high force needed to penetrate a DPPC membrane in the solid-like phase. Note that this force is similar to the force needed to indent an alkali halide single crystal (35), thus highlighting the strong lateral interactions created between two ordered neighboring phospholipid molecules. Indeed, force experiments on DPPC bilayers were performed with a stiffer cantilever (0.5 N/m) to reach the yield threshold force point. On increasing temperature, still in the solid-like phase, we observe a decrease in the yield threshold force. This decrease could be accounted for by the increase in the area/lipid value with temperature, which is in accordance with the surface mobility (defects disappearance) observations upon AFM images (Fig. 5, a and b). Thus, the higher the area per lipid value (less compact structure, reduced lateral interaction between neighboring molecules), the easier for the AFM tip to penetrate the bilayer. The yield threshold force reaches its minimum ($\sim 5\text{--}7\text{ nN}$) at $\sim 46^\circ\text{C}\text{--}50^\circ\text{C}$. Further increasing temperature within the liquid-like phase does not seriously affect the yield threshold force value. It

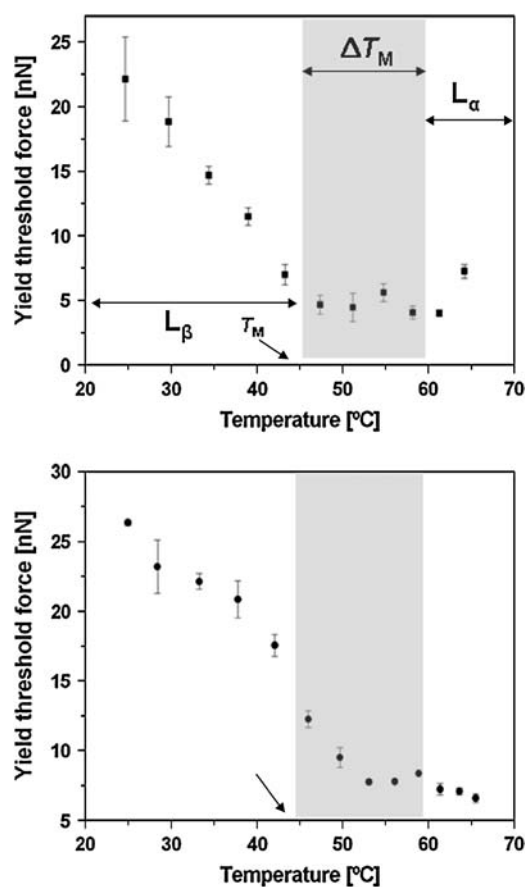


FIGURE 6 Yield threshold force dependence of a mica-supported DPPC bilayer with temperature for two independent experiments (different tip, different sample). All measurements were performed under high ionic strength solution. Each point in the graph corresponds to the center value of a Gaussian fitting to the obtained histogram. Error bars stand for standard deviation of the Gaussian fitting to the yield threshold force histograms. T_M stands for the main transition temperature obtained from DSC measurements. Dark areas stand for the temperature range (ΔT_M) in which phase transitions are observed in supported planar bilayers through AFM images (Fig. 5).

varies around an average value of $\sim 6\text{ nN}$. Dark areas in Fig. 6 account for the temperature range in which phase transition has been observed in mica-supported DPPC bilayers thanks to AFM contact images. In conclusion, we have observed that for DPPC-supported bilayers, i), solid-like phase presents a higher mechanical stability than fluid-like phase (the yield threshold force being up to threefold greater in the L_β phase region than in the L_α region for temperatures 20°C below the main transition temperature); ii), within the solid-like phase, yield threshold value decreases with increasing temperature. This process may be accounted for by the reduction in area/lipid value of the DPPC bilayer as temperature is increased, thus lowering lateral interaction between neighboring molecules; and iii), the lower yield threshold values occur also for DPPC bilayers in the temperature range where phase transitions are taking place, yielding very similar results to those obtained for DMPC bilayers.

Force spectroscopy on a DLPC bilayer

The two studied lipid bilayers have a high T_M , allowing us to make a quantitative comparison of the evolution of the yield threshold value between the gel and the liquid phase. To conclude with, we have studied the nanomechanical behavior of a DLPC bilayer, with a T_M value at a much lower temperature (-1°C). Therefore, we are dealing with the liquid phase at temperatures well above ($20\text{--}60^\circ\text{C}$) T_M . Fig. 7 *a* shows a $5 \times 5 \mu\text{m}^2$ contact mode AFM image of the totally covered surface acquired at 25°C . Here again in $>80\%$ of the recordings, the jump in the force plot has been observed, despite the liquid nature of the bilayer. An example is shown in Fig. 7 *b*, where a force-distance curve for a DLPC bilayer is observed. The yield threshold is pointed with an arrow. The evolution of the yield threshold force with temperature for two independent experiments (different tips, different samples) is shown in Fig. 7, *c* and *d*. At 23°C the yield

threshold is observed at ~ 9 nN. Increasing temperature yields to a decrease in the yield threshold force until reaching a minimum value at $\sim 35^\circ\text{C}$ (~ 5 nN). Surprisingly, at higher temperatures the yield threshold force started to increase until reaching maximum values at the higher sampled temperatures ($\sim 11\text{--}13$ nN at $60\text{--}65^\circ\text{C}$). This unexpected, reproducible behavior is indeed difficult to interpret, although a possible explanation is discussed below.

A different effect of ion binding on the nanomechanical response of the bilayer in the L_α and L_β phases

Up to this moment we have dealt with the evolution of the nanomechanics of supported lipid bilayers with temperature. All the experiments were performed under high ionic strength solutions (150 mM NaCl + 20 mM MgCl_2 , pH =

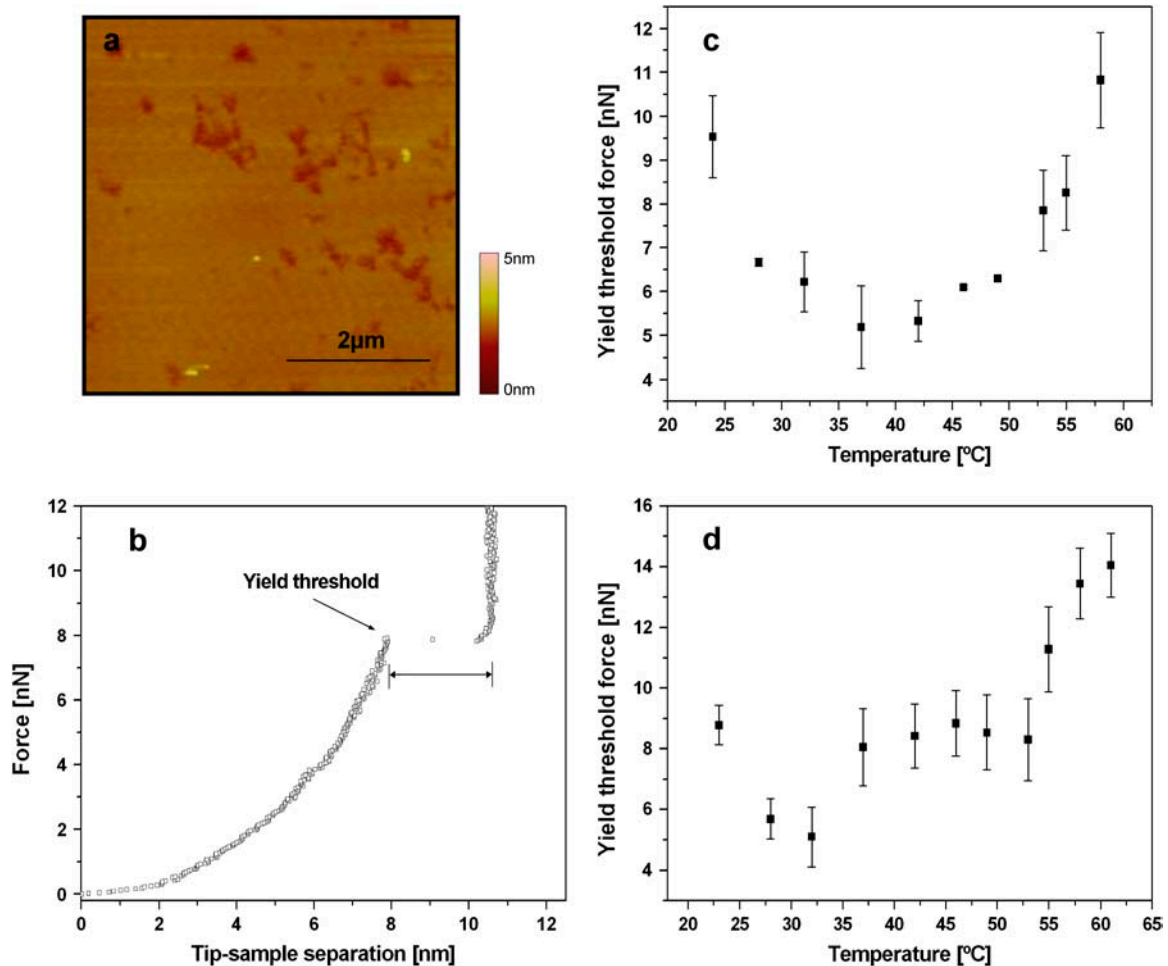


FIGURE 7 (a) $5 \times 5 \mu\text{m}^2$ contact mode AFM image of DLPC-supported bilayer showing total surface coverage. Force plots were performed in different positions all around the surface, yielding force-distance curves such as that observed in *b*, where the discontinuity in the curve is shown (yield threshold point). (c and d) Yield threshold force dependence of a mica-supported DLPC bilayer with temperature for two independent experiments (different tip, different sample). Each point in the graph corresponds to the center value of a Gaussian fitting to the obtained histogram. Error bars stand for standard deviation of the Gaussian fitting to the yield threshold force histograms. All measurements are performed in the liquid-like phase, since T_M (-1°C) is far below the sampled temperatures.

7.4), mainly because i), these experimental conditions mimic physiological conditions, and also because ii), ionic strength plays a key role upon bilayer deposition onto a mica surface (17). However, ionic strength (ion-binding effect) plays a key role in membrane nanomechanics. This fact has been recently observed through MD simulations (49,52–56) and also addressed by us in a recent work (1). However, most of these MD simulations were performed in the liquid-like phase for the studied phospholipid bilayers. We now have the chance of experimentally studying the role of ionic strength on both the solid-like and the liquid-like phases and to quantitatively compare the nanomechanical effect of cation binding within the two different phases for the same phospholipid molecule. Although the role of ionic strength has been previously addressed for the solid-like phase (1), showing a great increase of the yield threshold value as ionic strength was added to the measuring system, the effect of ion-binding on the nanomechanics of the system has not been studied in the fluid-like phase. Fig. 8 *a* shows the evolution of the yield threshold force with temperature for a DMPC-supported bilayer formed and measured under high ionic strength conditions (Fig. 8 *a*, black circles) and formed and measured in buffered water (white circles). Both experiments were conducted with the same tip. Although the trend is similar for both curves (both showing the well), the curve obtained for the bilayer measured in water is clearly shifted to lower force values, thus indicating that ionic strength has an effect on both the solid and the liquid phases. However, the yield threshold force difference within the solid phase (vertical left arrow) is much higher ($\Delta F_y = \sim 9$ nN) than the difference found within the liquid phase ($\Delta F_y = \sim 3$ nN), (vertical right arrow). Similar results were found when comparing the yield threshold force evolution for a DPPC bilayer (Fig. 8 *b*) when it was formed and measured under higher strength conditions (black circles) and in distilled water (white circles). Within the solid-like phase (vertical left arrow), the yield threshold force difference appears to be quite constant within the temperature range 22°C–42°C ($\Delta F_y = \sim 13$ –15 nN) and higher than the observed difference within the liquid-like phase ($\Delta F_y = \sim 1.5$ –2.5 nN). Therefore, we come to the conclusion that, even though ion binding seems to have an effect both in the liquid and gel phase, it is in the gel phase where its role is enhanced the most.

DISCUSSION

A full interpretation of the obtained results is not straightforward. A first qualitative approach could be made in terms of A (area per molecule) values. Indeed, the A values are known to be smaller (more packed structures) for the gel phase than for the liquid-like phase. Therefore, whereas $A = 47.2 \pm 0.5 \text{ \AA}^2$ for fully hydrated DMPC bilayers at 10°C (gel phase) (44), it turns out to be $A = 60.6 \pm 0.5 \text{ \AA}^2$ for fully hydrated fluid phase at 30°C (57), resulting in a reduction of the 22%

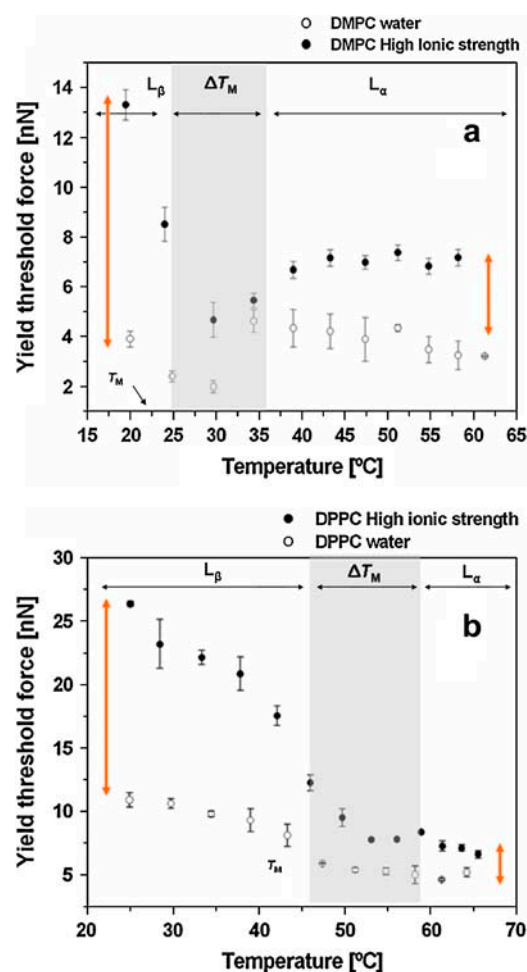


FIGURE 8 Yield threshold force dependence with temperature of a mica-supported (a) DMPC bilayer and (b) DPPC bilayer formed and measured in buffered distilled water (white circles) and in buffered high ionic strength solution (black circles). In both cases both curves exhibit a well around the surface transition temperature ΔT_M (darker region), and the bilayer measured under high ionic strength conditions is shifted to higher yield force values, thus suggesting a higher stiffness, both in the solid-like and in the liquid-like phases. The difference in the yield threshold force is enhanced in the solid-state phase (left arrows) with respect to the liquid-like phase (right arrows). Both curves (under high ionic strength and distilled water) for DMPC and DPPC were performed with the same tip ($k_c = 0.08$ N/m for DMPC and $k_c = 0.5$ N/m for DPPC).

in the gel phase with respect to the liquid phase. A similar trend is observed for DPPC bilayers, yielding $A = 47.9 \text{ \AA}^2$ for the gel phase (20°C) and $A = 64 \text{ \AA}^2$ for the fluid phase (50°C) (2). A more packed structure results in an increase of the order parameter and to an enhancement of lateral interactions between neighboring groups. As a consequence, the observed experimental trend (a higher resistance of the whole phospholipids network upon breakthrough in the gel phase and a decrease of the yield threshold value in the liquid phase) is in good accordance with area per lipid values considerations. This simple interpretation can qualitatively explain both the difference in yield threshold value between

the solid phase and the liquid phase for a given phospholipid (DMPC and DPPC) and also within the solid phase (in the case of DPPC). Nonetheless, there are two features in the yield threshold force versus temperature plots that cannot be explained only in terms of increasing the lateral area per lipid values from the gel phase to the fluid phase. On the one hand, the graphs corresponding to DMPC (Fig. 4) and to DPPC (Fig. 6) show a minimum in the yield threshold force at temperatures close to their T_M . On the other hand, and especially in the case of DLPC (Fig. 7), the yield threshold value increases at high temperatures ($T > 50^\circ\text{C}$ in the case of DLPC) after a deep well.

Concerning the first issue, it is clear that the membrane is easier to be punctured (i.e., becomes “softer”, the breakthrough event occurs at lower forces) at temperatures close to the main transition temperature, resulting in a well in the graph. Therefore, it could also be considered that around the T_M , the membrane exhibits an “anomalous” softening mechanical behavior. In fact, many physical quantities have been found to display an anomalous behavior around T_M , such as heat capacitance, ζ -potential (4), electric conductivity (5), Na^+ permeability (6), NMR order parameter (7), or swelling (8). The latter is especially interesting since it has been reported by various groups and is directly related to structural and mechanical characteristics. The experimental observation that with decreasing temperature, fluid-like, L_α , DMPC and DPPC bilayers exhibit a nonlinear increase in their lamellar repeat spacing, d , of 3–5 Å, is known as “anomalous swelling” (58). The origin of such swelling has been a matter of scientific discussion for years, although the most recent contributions tend to assess that it is the expansion of the water layer (d_w) rather than an expansion of the hydrophilic phosphatidylcholine headgroup or an anomalous expansion of the hydrophobic tail, the last responsible for this unexpected thickness increase (8). After excluding the possibility that the anomalous expansion of d_w could be attributed to changes in either the hydration or the van der Waals force, Pabst and co-workers (8) came to the conclusion through the measurement of the Caillé fluctuation parameter (η_1) in multilamellar vesicles that the expansion of d_w is due to steric repulsion of bilayers caused by increased fluctuations. Similar conclusions were reached upon NMR ^2H measurements, which have shown an “anomalous disordering” of the interbilayer water around the main phase transition (7,59). These observations, together with osmotic pressure studies, conclude that bilayers soften in the vicinity of T_M , experiencing increased levels of repulsion. Overall, these anomalies strongly suggest that lipid bilayers undergo a significant structural rearrangement in the headgroup and in the acyl chain regions around the main transition. Interbilayer water and hydration processes seem to play a key role upon membrane structural stability and seem to be strongly correlated to the ordering in the headgroups as electron spin resonance experiments confirm (9). Indeed, recent MD simulation results demonstrate that 76% of DMPC mole-

cules in the bilayer are linked by single or multiple water bridges (60) and that DMPC headgroups also interact directly via Coulombic interaction between negatively charged phosphate or carbonyl oxygen atoms of another molecule. Those two short-range interactions present in the liquid-crystalline phase give rise to long-lived clusters that form an extended network of interactions among PC groups (61). These interactions link 98% of all PC molecules in the membrane, thus highlighting the role of PC headgroup-headgroup interactions in the stability of the membrane. Besides, the presence of cations within the headgroup network is likely to enhance even more such interactions between neighboring headgroups (49,52,61). In any case, and even in the absence of salt, for the reasons outlined above, it seems clear that water plays a key role in membrane stability. Besides ^2H NMR measurements (that pointed out the reduction in interbilayer water ordering at the main phase transition and interpreted this fact in terms of a coupling between fluctuations in interbilayer water concentration and lateral density fluctuations in the headgroup region), ESR measurements show that ordering of the headgroups and ordering of the interbilayer water are correlated (which is consistent with the membrane picture revealed by MD simulations). Furthermore, these results suggest that both ordering of the headgroups and of the interbilayer water are inversely correlated with the degree of hydration of lipid bilayers. At T_M , the ordering of headgroups and the ordering of interbilayer water are the lowest, and the swelling of the bilayers reaches their maximum by increasing hydration of headgroups near the main phase transition, taking into account that dehydration or hydration of bilayers is a dynamic process of water moving between the interbilayer region and the bulk water phase. This result is consistent with the decrease in the yield threshold force observed upon ethanol addition to the measuring solution (1) that is known to decrease interbilayer water ordering (62).

Besides interbilayer water and hydration of the polar groups, several studies have been conducted regarding the structure of the hydrocarbon chains of phospholipid bilayers around T_M and its effect on the mechanical behavior of PC bilayers (63,64). More precisely, measurements of properties such as bending rigidity (K_c) (8) have concluded that a softening of the bilayer takes place around T_M (65). Lee et al. (66) detected a decrease in K_c studying DPPC vesicles at variable temperatures by means of optical methods around DPPC transition temperature. This fact had been previously reported by Heimburg et al. (67) by using Monte Carlo simulations to study the mechanics of DPPC bilayers. This K_c variation was attributed to a hydrocarbon-chain melting around T_M . Previous works performed by Needham and Evans (68,69) on the mechanics of giant vesicles suspended on glass micropipettes highlighted the key role of hydrocarbon-chain disorder in the DMPC vesicles transition process. They found an increase of the surface shear viscosity while decreasing temperature from liquid phase through T_M until

reaching gel phase, showing the softening of the bilayer around T_M . Measurements of the widths of the bilayers in different phases led us to conclude that there is some degree of rotameric chain disorder as the bilayer approaches its T_M . This panorama borne in mind, it seems quite clear that around the T_M hydrocarbon chain, headgroup and interbilayer water, a key element upon membrane stability, present the lowest ordering, which is again increased at lower and upper temperatures. Around T_M , thus, the AFM tip can penetrate the bilayer easier, and this is reflected in the lower yield threshold force observed in Figs. 4 and 6.

The second striking experimental observation is that the yield threshold force increases at high temperatures ($T > 50^\circ\text{C}$) for DLPC. Of course, in the whole range of temperatures, DLPC is in the L_α phase. Therefore, due to the enhancement of steric fluctuations and the increase of the lateral area/lipid value with temperature, one would expect a decrease of the yield threshold force with temperature. This trend is accomplished for temperatures 20–45°C. However, as temperature is further increased, the yield threshold force increases. This experimental feature has been observed for >10 individual temperature ramp series using different samples and different tips, and the obtained results have been always reproducible. This experimental trend is presently lacking interpretation. There is, however, an extra parameter that could (partially) account for this fact. Although the thickness of the interbilayer water increases with temperature, the membrane thickness, d_B , decreases with temperature (8,70). Therefore, the absolute value of the linear thermal expansion coefficient, α , decreases linearly at high temperatures (from 70°C to 40°C in the case of 1-palmitoyl-2-oleoyl-*sn*-glycero-3-phosphocholine (POPC)), indicating reduced bilayer elasticity (70). In this case, then, the reduced hydrocarbon chain elasticity term (higher bilayer stiffness) would dominate over the entropic fluctuation term at temperatures far above T_M , and it would be, therefore, the hydrophobic chain that is mainly responsible for membrane stability rather than the less-ordered headgroup moiety. Additional future work on this particular issue may help to shed light onto this question.

Regarding the role of ions upon membrane stability, recent MD simulation results have demonstrated (49,52,53) that the presence of cations (such as in the results presented here, namely, Na^+ and Ca^{2+}) in the phospholipids network would change drastically the structural and dynamical properties of the PC membranes. On average, every Na^+ cation binds to three carbonyl oxygens and to 1–2 water oxygens. Due to their threefold increased size as compared to single lipids, these complexes are less mobile. As a consequence, a decrease in the average area per lipid from 0.655 nm² to 0.606 nm² (>8%) is observed for POPC when Na^+ cations are introduced in the system, giving rise to a more compact overall structure. Indeed, the difference in the area per group is also reflected by the ordering of the lipid hydrocarbon tails (49,53). A similar case applied to Ca^{2+} , each Ca^{2+} cation

binding to 4.2 PC heads on average. Therefore, and according to those MD simulations, the higher order structure promoted by ions on the bilayer, which give rise to a reduction in average area per lipid (higher compactness) and to a more rigid structure (lower diffusion coefficient), may be the cause for the higher membrane stability experimentally observed through the nanomechanical response of the system obtained by force spectroscopy measurements (1). In this work, we extend these results, mainly performed on the gel phase, to the liquid-like phase, and we confirm that indeed ion binding gives rise to a higher yield threshold force value within the whole range of sampled temperatures. However, the increase in yield threshold force due to the presence of ions in the measuring solution is much more evident in the gel phase than in the liquid-like phase, probably due to the lower distance between the neighboring phospholipid molecules forming the bilayer in the gel phase, which allows cations to enhance even more lateral interactions between neighboring molecules.

CONCLUSIONS

The effect of temperature on the nanomechanical properties of supported lipid bilayers has been experimentally studied by force spectroscopy in a quantitative way. We have related the evolution of the force required to penetrate the bilayer with an AFM tip (which is a direct measure of bilayer compactness) with the structural phase transitions observed upon AFM contact images. The main phase transition ($L_\beta \rightarrow L_\alpha$) takes place in supported bilayers within a range of temperatures of ~10–13°C. Phase transitions have indeed a clear mechanical effect on the stability of the bilayer. As expected, the solid-like phase shows a much higher resistance upon breakthrough than the fluid-like phase as proved for DMPC- and DPPC-supported bilayers. Besides, although temperature has a strong effect on the nanomechanics of the solid-like phase, it does not have such a huge impact on the yield threshold value in the liquid-like phase, at least for a temperature range of 10–60°C above T_M . Interestingly, the yield force versus temperature plot shows a well for temperatures around T_M (in close relationship with AFM images), and hence an anomalous mechanical softening behavior has been assessed. This unexpected behavior around T_M has also been widely reported for many physical quantities, thus indicating that the membrane undergoes important structural changes within this temperature range. The interpretation of the nanomechanical response of the system within this temperature range has been performed in light of the new available data provided with MD simulations, which outline the role of water upon membrane mechanical stability and also according to data provided with other experimental techniques, mainly performed with multilamellar systems and we are now relating them to single supported bilayers. Our results experimentally corroborate the predictions that the membrane softens around

T_M on account of enhanced steric repulsions because of the decrease in headgroup ordering and also because of the disorder induced in the hydrocarbon chains in the vicinity of T_M . The anomalous trend observed for DLPC at high temperatures still lacks full interpretation, although the increase of bilayer stiffness at high temperatures could partially account for the observed experimental results.

Last but not least, the role of ion binding upon membrane stability within the two different phases has also been discussed, suggesting that although ion binding increases the yield threshold force within all ranges of temperature (and different phases), it is in the gel phase where this effect is more outstanding. Summarizing, this work shows how temperature-governed structural processes can have a mechanical response at the nanometer/nanonewton scale and how phase transitions have mechanical implications. It also highlights the use of temperature-controlled AFM for the study of biologically relevant issues that are temperature dependent at the nanometer scale.

SUPPLEMENTARY MATERIAL

An online supplement to this article can be found by visiting BJ Online at <http://www.biophysj.org>.

We thank Dr. Jordi Hernandez-Borrell (UB) and Dr. Antoni Morros (UAB) for kindly allowing us to use the DSC equipment and also Òscar Domènech for helpful discussions.

S.G.-M. thanks Departament d'Universitats, Recerca i Societat de la Informació (DURSI) (Generalitat de Catalunya) for a grant, and we all thank DURSI (Generalitat de Catalunya) for financial support through projects 2000SGR017 and AGP99-10.

REFERENCES

- Garcia-Manyes, S., G. Oncins, and F. Sanz. 2005. Effect of ion-binding and chemical phospholipid structure on the nanomechanics of lipid bilayers studied by force spectroscopy. *Biophys. J.* 89:1812–1826.
- Nagle, J. F., and S. Tristram-Nagle. 2000. Structure of lipid bilayers. *Biochim. Biophys. Acta.* 1469:159–195.
- Nagle, J. F., H. I. Petrache, N. Gouliavov, S. Tristram-Nagle, Y. F. Liu, R. M. Suter, and K. Gawrisch. 1998. Multiple mechanisms for critical behavior in the biologically relevant phase of lecithin bilayers. *Phys. Rev.* 58:7769–7776.
- Makino, K., T. Yamada, M. Kimura, T. Oka, H. Ohshima, and T. Kondo. 1991. Temperature- and ionic strength-induced conformational changes in the lipid head group region of liposomes as suggested by zeta potential data. *Biophys. Chem.* 41:175–183.
- Wu, S. H. W., and H. M. McConnell. 1973. Lateral phase separations and perpendicular transport in membranes. *Biochem. Biophys. Res. Commun.* 55:484–491.
- Papahadjopoulos, D., K. Jacobson, S. Nir, and T. Isac. 1973. Phase transitions in phospholipid vesicles. Fluorescence polarization and permeability measurements concerning the effect of temperature and cholesterol. *Biochim. Biophys. Acta.* 311:330–348.
- Pope, J. M., L. Walker, B. A. Cornell, and G. W. Francis. 1981. NMR study of synthetic lecithin bilayers in the vicinity of the gel-liquid-crystal transition. *Biophys. J.* 35:509–520.
- Pabst, G., J. Katsaras, V. A. Raghunathan, and M. Rappolt. 2003. Structure and interactions in the anomalous swelling regime of phospholipid bilayers. *Langmuir.* 19:1716–1722.
- Ge, M., and J. H. Freed. 2003. Hydration, structure, and molecular interactions in the headgroup region of dioleoylphosphatidylcholine bilayers: an electron spin resonance study. *Biophys. J.* 85:4023–4040.
- Leonenko, Z. V., A. Carnini, and D. T. Cramb. 2000. Supported planar bilayer formation by vesicle fusion: the interaction of phospholipid vesicles with surfaces and the effect of gramicidin on bilayer properties using atomic force microscopy. *Biochim. Biophys. Acta.* 1509:131–147.
- Jass, J., T. Tjarnhage, and G. Puu. 2000. From liposomes to supported, planar bilayer structures on hydrophilic and hydrophobic surfaces: an atomic force microscopy study. *Biophys. J.* 79:3153–3163.
- Sackmann, E. 1996. Supported membranes: scientific and practical applications. *Science.* 271:43–48.
- Benz, M., T. Gutschmann, N. Chen, R. Tadmor, and J. Israelachvili. 2004. Correlation of AFM and SFA measurements concerning the stability of supported lipid bilayers. *Biophys. J.* 86:870–879.
- Kaasgaard, T., C. Leidy, J. H. Ipsen, O. G. Mouritsen, and K. Jorgensen. 2001. In situ atomic force microscope imaging of supported lipid bilayers. *Single Molecules.* 2:105–108.
- Schneider, J., Y. F. Dufrene, W. R. Barger Jr., and G. U. Lee. 2000. Atomic force microscope image contrast mechanisms on supported lipid bilayers. *Biophys. J.* 79:1107–1118.
- Schneider, J., W. Barger, and G. U. Lee. 2003. Nanometer scale surface properties of supported lipid bilayers measured with hydrophobic and hydrophilic atomic force microscope probes. *Langmuir.* 19:1899–1907.
- Egawa, H., and K. Furusawa. 1999. Liposome adhesion on mica surface studied by atomic force microscopy. *Langmuir.* 15:1660–1666.
- Silin, V. I., H. Wieder, J. T. Woodward, G. Valincius, A. Offenhausser, and A. L. Plant. 2002. The role of surface free energy on the formation of hybrid bilayer membranes. *J. Am. Chem. Soc.* 124:14676–14683.
- Zasadzinski, J. A. N., C. A. Helm, M. L. Longo, A. L. Weisenhorn, S. A. C. Gould, and P. K. Hansma. 1991. Atomic force microscopy of hydrated phosphatidylethanolamine bilayers. *Biophys. J.* 59:755–760.
- Egger, M., F. Ohnesorge, A. L. Weisenhorn, S. P. Heyn, B. Drake, C. B. Prater, S. A. C. Gould, P. K. Hansma, and H. E. Gaub. 1990. Wet lipid protein membranes imaged at submolecular resolution by atomic force microscopy. *J. Struct. Biol.* 103:89–94.
- Hansma, H. G., A. L. Weisenhorn, A. B. Edmundson, H. E. Gaub, and P. K. Hansma. 1991. Atomic force microscopy—seeing molecules of lipid and immunoglobulin. *Clin. Chem.* 37:1497–1501.
- Butt, H. J., E. K. Wolff, S. A. C. Gould, B. D. Northern, C. M. Peterson, and P. K. Hansma. 1990. Imaging cells with the atomic force microscope. *J. Struct. Biol.* 105:54–61.
- Leonenko, Z. V., E. Finot, H. Ma, T. E. Dahms, and D. T. Cramb. 2004. Investigation of temperature-induced phase transitions in DOPC and DPPC phospholipid bilayers using temperature-controlled scanning force microscopy. *Biophys. J.* 86:3783–3793.
- Giocondi, M. C., and C. Le Grimellec. 2004. Temperature dependence of the surface topography in dimyristoylphosphatidylcholine/distearoylphosphatidylcholine multibilayers. *Biophys. J.* 86:2218–2230.
- Enders, O., A. Ngezahayo, M. Wiechmann, F. Leisten, and H. A. Kolb. 2004. Structural calorimetry of main transition of supported DMPC bilayers by temperature-controlled AFM. *Biophys. J.* 87:2522–2531.
- Seantier, B., C. Breffa, O. Felix, and G. Decher. 2004. In situ investigations of the formation of mixed supported lipid bilayers close to the phase transition temperature. *Nano Lett.* 4:5–10.
- Tokumasu, F., A. J. Jin, and J. A. Dvorak. 2002. Lipid membrane phase behaviour elucidated in real time by controlled environment atomic force microscopy. *J. Electron Microscop.* (Tokyo). 51:1–9.
- Giocondi, M. C., L. Pacheco, P. E. Milhiet, and C. Le Grimellec. 2001. Temperature dependence of the topology of supported dimyristoyl-distearoyl phosphatidylcholine bilayers. *Ultramicroscopy.* 86:151–157.

29. Weisenhorn, A. L., P. Maivald, H. J. Butt, and P. K. Hansma. 1992. Measuring adhesion, attraction, and repulsion between surfaces in liquids with an atomic-force microscope. *Phys. Rev. B.* 45:11226–11232.
30. Jaschke, M., H. J. Butt, H. E. Gaub, and S. Manne. 1997. Surfactant aggregates at a metal surface. *Langmuir.* 13:1381–1384.
31. O'Shea, S. J., and M. E. Welland. 1998. Atomic force microscopy at solid-liquid interfaces. *Langmuir.* 14:4186–4197.
32. O'Shea, S. J., M. E. Welland, and T. Rayment. 1992. Solvation forces near a graphite surface measured with an atomic force microscope. *Appl. Phys. Lett.* 60:2356–2358.
33. Franz, V., and H. J. Butt. 2002. Confined liquids: solvation forces in liquid alcohols between solid surfaces. *J. Phys. Chem. B.* 106:1703–1708.
34. Sun, G. X., E. Bonaccorso, V. Franz, and H. J. Butt. 2002. Confined liquid: simultaneous observation of a molecularly layered structure and hydrodynamic slip. *J. Chem. Phys.* 117:10311–10314.
35. Fraxedas, J., S. Garcia-Manyes, P. Gorostiza, and F. Sanz. 2002. Nanoindentation: toward the sensing of atomic interactions. *Proc. Natl. Acad. Sci. USA.* 99:5228–5232.
36. Dufrene, Y. F., T. Boland, J. W. Schneider, W. R. Barger, and G. U. Lee. 1998. Characterization of the physical properties of model biomembranes at the nanometer scale with the atomic force microscope. *Faraday Discuss.* 111:79–94.
37. Richter, R. P., and A. Brisson. 2003. Characterization of lipid bilayers and protein assemblies supported on rough surfaces by atomic force microscopy. *Langmuir.* 19:1632–1640.
38. Franz, V., S. Loi, H. Müller, E. Bamberg, and H. J. Butt. 2002. Tip penetration through lipid bilayers in atomic force microscopy. *Colloids Surf. B Biointerfaces.* 23:191–200.
39. Loi, S., G. Sun, V. Franz, and H. J. Butt. 2002. Rupture of molecular thin films observed in atomic force microscopy. II. Experiment. *Phys. Rev.* 66:031602.
40. Butt, H. J., and V. Franz. 2002. Rupture of molecular thin films observed in atomic force microscopy. I. Theory. *Phys. Rev.* 66:031601.
41. Mueller, H., H. J. Butt, and E. Bamberg. 2000. Adsorption of membrane-associated proteins to lipid bilayers studied with an atomic force microscope: myelin basic protein and cytochrome c. *J. Phys. Chem. B.* 104:4552–4559.
42. Florin, E. L., M. Rief, H. Lehmann, M. Ludwig, C. Dornmair, V. T. Moy, and H. E. Gaub. 1995. Sensing specific molecular-interactions with the atomic-force microscope. *Biosens. Bioelectron.* 10:895–901.
43. Proksch, R., T. E. Schaffer, J. P. Cleveland, R. C. Callahan, and M. B. Viani. 2004. Finite optical spot size and position corrections in thermal spring constant calibration. *Nanotechnology.* 15:1344–1350.
44. Tristram-Nagle, S., Y. Liu, J. Legleiter, and J. F. Nagle. 2002. Structure of gel phase DMPC determined by x-ray diffraction. *Biophys. J.* 83:3324–3335.
45. Yang, J., and J. Appleyard. 2000. The main phase transition of mica-supported phosphatidylcholine membranes. *J. Phys. Chem. B.* 104:8097–8100.
46. Nagle, J. F. 1975. Chain model theory of lipid monolayer transitions. *J. Chem. Phys.* 63:1255–1261.
47. Oncins, G., S. Garcia-Manyes, and F. Sanz. 2005. Study of frictional properties of a phospholipid bilayer in a liquid environment with lateral force microscopy as a function of NaCl concentration. *Langmuir.* 21:7373–7379.
48. Sturtevant, J. M. 1998. The effect of sodium chloride and calcium chloride on the main phase transition of dimyristoylphosphatidylcholine. *Chem. Phys. Lipids.* 95:163–168.
49. Bockmann, R. A., A. Hac, T. Heimburg, and H. Grubmuller. 2003. Effect of sodium chloride on a lipid bilayer. *Biophys. J.* 85:1647–1655.
50. Israelachvili, J. N. 1991. Intermolecular and Surface Forces: With Applications to Colloidal and Biological Systems. Academic Press, London.
51. Pera, I., R. Stark, M. Kappl, H. J. Butt, and F. Benfenati. 2004. Using the atomic force microscope to study the interaction between two solid supported lipid bilayers and the influence of synapsin I. *Biophys. J.* 87:2446–2455.
52. Bockmann, R. A., and H. Grubmuller. 2004. Multistep binding of divalent cations to phospholipid bilayers: a molecular dynamics study. *Angew. Chem. Int. Ed. Engl.* 43:1021–1024.
53. Pandit, S. A., D. Bostick, and M. L. Berkowitz. 2003. Molecular dynamics simulation of a dipalmitoylphosphatidylcholine bilayer with NaCl. *Biophys. J.* 84:3743–3750.
54. Pandit, S. A., and M. L. Berkowitz. 2002. Molecular dynamics simulation of dipalmitoylphosphatidylserine bilayer with Na⁺ counterions. *Biophys. J.* 82:1818–1827.
55. Mukhopadhyay, P., L. Monticelli, and D. P. Tieleman. 2004. Molecular dynamics simulation of a palmitoyl-oleoyl phosphatidylserine bilayer with Na⁺ counterions and NaCl. *Biophys. J.* 86:1601–1609.
56. Sachs, J. N., H. Nanda, H. I. Petrache, and T. B. Woolf. 2004. Changes in phosphatidylcholine headgroup tilt and water order induced by monovalent salts: molecular dynamics simulations. *Biophys. J.* 86:3772–3782.
57. Kucerka, N., Y. Liu, N. Chu, H. I. Petrache, S. Tristram-Nagle, and J. F. Nagle. 2005. Structure of fully hydrated fluid phase DMPC and DLPC lipid bilayers using x-ray scattering from oriented multilamellar arrays and from unilamellar vesicles. *Biophys. J.* 88:2626–2637.
58. Mason, P. C., J. F. Nagle, R. M. Epanand, and J. Katsaras. 2001. Anomalous swelling in phospholipid bilayers is not coupled to the formation of a ripple phase. *Phys. Rev.* 63:030902.
59. Hawton, M. H., and J. W. Doane. 1987. Pretransitional phenomena in phospholipid/water multilayers. *Biophys. J.* 52:401–404.
60. Pasenkiewicz-Gierula, M., Y. Takaoka, H. Miyagawa, K. Kitamura, and A. Kusumi. 1997. Hydrogen bonding of water to phosphatidylcholine in the membrane as studied by a molecular dynamics simulation: location, geometry, and lipid-lipid bridging via hydrogen-bonded water. *J. Phys. Chem. A.* 101:3677–3691.
61. Pasenkiewicz-Gierula, M., Y. Takaoka, H. Miyagawa, K. Kitamura, and A. Kusumi. 1999. Charge pairing of headgroups in phosphatidylcholine membranes: a molecular dynamics simulation study. *Biophys. J.* 76:1228–1240.
62. Ho, C., and C. D. Stubbs. 1997. Effect of n-alkanols on lipid bilayer hydration. *Biochemistry.* 36:10630–10637.
63. Rawicz, W., K. C. Olbrich, T. McIntosh, D. Needham, and E. Evans. 2000. Effect of chain length and unsaturation on elasticity of lipid bilayers. *Biophys. J.* 79:328–339.
64. Olbrich, K., W. Rawicz, D. Needham, and E. Evans. 2000. Water permeability and mechanical strength of polyunsaturated lipid bilayers. *Biophys. J.* 79:321–327.
65. Dimova, R. I., C. Dietrich, and B. Pouligny. 2000. Viscoelasticity of DMPC-vesicle membranes near the main phase transition: optical trapping manipulation of latex beads. *Biophys. J.* 78:273A.
66. Lee, C. H., W. C. Lin, and J. Wang. 2001. All-optical measurements of the bending rigidity of lipid-vesicle membranes across structural phase transitions. *Phys. Rev. E.* 64:020901.
67. Heimburg, T. 2000. A model for the lipid pretransition: coupling of ripple formation with the chain-melting transition. *Biophys. J.* 78:1154–1165.
68. Evans, E., and D. Needham. 1987. Physical properties of surfactant bilayer membranes: thermal transitions, elasticity, rigidity, cohesion and colloidal interactions. *J. Phys. Chem.* 91:4219–4228.
69. Needham, D., and E. Evans. 1988. Structure and mechanical properties of giant lipid (DMPC) vesicle bilayers from 20°C below to 10°C above the liquid crystal-crystalline phase transition at 24°C. *Biochemistry.* 27:8261–8269.
70. Pabst, G., M. Rappolt, H. Amenitsch, S. Bernstorff, and P. Laggner. 2000. X-ray kinematography of temperature-jump relaxation probes the elastic properties of fluid bilayers. *Langmuir.* 16:8994–9001.